(Received 4 December 2025, Accepted 21 January 2026, Scheduled 12 February 2026)

A Low Sidelobe Dual-Beam Sparse Reflectarray Antenna with Combination of Transmissive and Reflective Elements

Wei Luo[1], Mingli Xie[1,*], Liu Luo[1], and Yuqi Yang[2]

[1]School of Electronic Science and Engineering, Chongqing University of Posts and Telecommunications, Chongqing 400065, China
[2]Electromagnetic Field and Wireless Technology Innovation Team, Chongqing University Posts and Telecommunications Chongqing 400065, China

ABSTRACT: A low side-lobe dual-beam reflectarray antenna is proposed based on the sparse array principle. The reflected dual beams achieve high gain through optimized phase compensation, in which the transmissive elements act as dummy elements to suppress side lobes. A global search optimization technique based on genetic algorithm (GA) is adopted to improve the arrangement of transmissive and reflection elements. Since all the reflective and transmissive elements operating in the same wide frequency band are non-uniformly distributed on the aperture, both the backward radiation and cross polarization levels are effectively suppressed. The measurement results show that the side-lobe level of the dual-beams is less than −19 dB. The peak gain and peak aperture efficiency of the designed antenna are 26.0 dBi and 38.9%, respectively. The 3-dB gain bandwidth is 13.8%. The front to back ratio at 30 GHz is 27 dB. This dual-beam antenna has the advantages of high gain, low side lobes, and wide beam radiation range, which make it suitable for millimeter-wave multi-target radar detection systems.

1. INTRODUCTION

Dual-beam antennas have garnered increasing academic and industrial interest within radar and satellite domains, owing to their capability of providing wide signal coverage and high communication capacity [1]. While low side-lobe antennas are applied in scenarios that are sensitive to interference, dual-beam antennas are more suitable for high-capacity, multi-user communication scenarios. The combination of the two antenna families can further optimize system performance to meet the strict requirements of modern communication, radar, and satellite Internet [2, 3].

Multiple beams can be achieved using geometrical partitioning or aperture field superposition methods [4]. In [5], a triple-beam metasurface antenna is designed by superimposing multiple aperture fields. A dual-beam transmitarray antenna (TA) using an ultra-thin Huygens phase-shifting unit was designed in [6], which adopts the phase superposition method. Owing to phase errors and vector field superposition, the side-lobe level (SLL) of dual-beam antennas is typically much higher than that of single-beam antennas with the same aperture size. In addition, frequency and polarization reuse techniques can be combined to create multiple beams with varied frequency bands and disparate polarization states [7, 8]. Owing to the mutual interference between beams of different frequencies and polarizations, the SLL and cross polarization levels of such antennas are relatively high.

Low-SLL antennas have important application value in radar detection systems and satellite communication, as they can effectively reduce interference and enhance communication concealment [9–12]. Amplitude-phase adjustable metasurfaces are commonly used in low side-lobe antennas. An amplitude-phase-controlled reflectarray combines a Taylor distribution to regulate the amplitude of electromagnetic (EM) waves to suppress the side lobes of the reflectarray antenna (RA) [13]. In [14], a method to reduce the SLL of a dual-beam RA was proposed, which used a reflective metasurface for amplitude compensation and combined Schelkunoff polynomials to reduce the side-lobe radiation of multiple beams. A technique combining Taylor distribution with dual-medium and Gaussian filtering is proposed in [15] to mitigate the gain loss caused by amplitude regulation. RA with low side lobes often uses reflective metasurfaces based on polarization conversion units, which convert a co-polarized wave into a cross-polarized wave by amplitude modulation, thereby increasing the cross-polarization level. Combining the theory of sparse arrays with metasurface layouts can achieve a low SLL, which can enhance the radiation performance of the RA [16, 17].

A low side-lobe dual-beam RA is proposed, which consists of a feeder and a metasurface integrated with transmissive and reflection elements, as shown in Fig. 1. Drawing on the idea of a sparse array antenna, a genetic algorithm (GA) was used to optimize the arrangement of transmissive and reflection elements to reduce the SLL of the reflected beam. The amplitude of the reflection is regulated with a unit distribution, without polarization conversion loss. The directions of the two beams are (0°, 30°) and (0°, −30°), respectively. The features of high gain and low SLL indicate that the proposed antenna is suitable for multi-target radar-detection systems.

* Corresponding author: Mingli Xie (2524009817@qq.com).

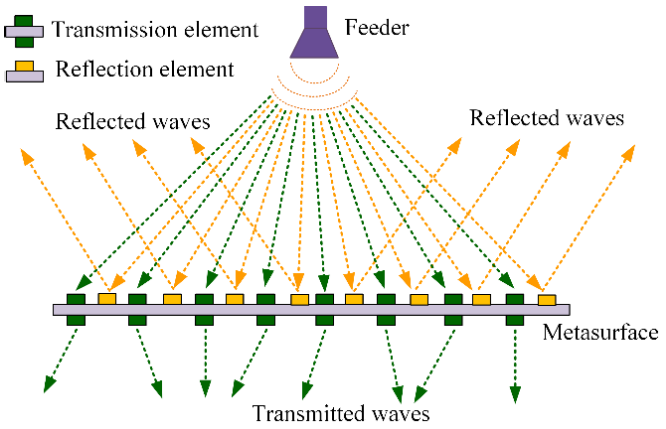

FIGURE 1. Schematic of the dual-beam sparse array antenna structure based on transmissive and reflective elements.

2. DESIGN OF THE PHASE ELEMENT

Because both the receiving-transmitting and reflective elements have a metallic structure, using the transmissive elements of the receiving-transmitting structure to regulate EM waves can reduce the impact of the transmitting elements on the performance of the reflective elements.

2.1. Analysis of the Transmissive Element

Transmissive element 1, as shown in Fig. 2, was designed, which includes three metal layers separated by F4B dielectric interlayers ($\varepsilon_r = 3.5$, $\tan\delta = 0.001$) characterized by a thickness of 1.4 mm. The receiving structure in the top layer and the transmitting structure in the bottom layer were connected by a metallic via to transmit EM waves. The receiving and transmitting structures have the same structural parameters. To avoid short circuits, the diameter of the circular hole in the center of the ground was slightly larger than that of the metallic via. Transmissive element 2 is obtained by rotating the bottom transmitting structure around the metallic surface at 180° based on transmitting element 1.

The co-polarized transmissive coefficient T_{yy} of the two transmissive elements under the vertical incidence of the y-polarized EM waves is shown in Fig. 3(a). Both T_{yy} amplitudes are better than 0.9 at 30 GHz. The influence of the oblique incidence angle of the EM waves on T_{yy} is shown in Fig. 3(b). When the oblique incidence angle of the EM waves is less than 35°, the amplitude and phase of T_{yy} remain almost unchanged. Thus, the focal length F should be reasonably selected to ensure that the incident angle of EM waves for each transmissive element is less than 35°.

2.2. Analysis of the Reflective Element

As shown in Fig. 4, the reflective element was designed to regulate the reflected EM waves, which was composed of a metal resonant layer, upper dielectric substrates, ground, and bottom dielectric substrates. A metal resonant layer was used to control the phase of the reflected EM waves, and the ground was used to reflect EM waves from the feeder. Compared with the traditional reflective elements with a metal-dielectric-metal structure, this reflective element has an additional layer of lower dielectric, and the thicknesses of the dielectric substrates of the reflection element and transmissive element are the same. The double-layer dielectric design guarantees the uniform thickness of the entire metasurface regardless of the arrangement pattern of transmissive and reflective elements across the aperture, regardless of the arrangement of the transmissive and reflection elements on the aperture.

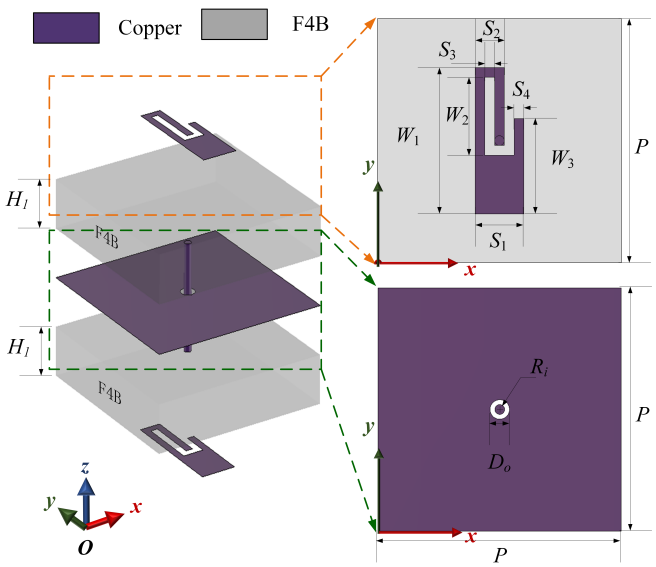

FIGURE 2. Breakdown view of the transmissive element structure ($P = 5.00$, $S_1 = 1.00$, $S_2 = 0.60$, $S_3 = 0.20$, $S_4 = 0.20$, $W_1 = 3.00$, $W_2 = 1.55$, $W_3 = 2.05$, $R_i = 0.10$, $D_o = 0.40$, $H_1 = 1.40$, unit: mm).

The phase of the reflected EM waves can be manipulated by adjusting the structural parameter L, thereby achieving directional control of the reflected beam. As illustrated in Fig. 5(a), the phase coverage of R_{yy} (the co-polarized reflection coefficient under y-polarized incident waves) reaches 300° from 26 GHz to 32 GHz, as L varies from 0.2 to 2.2 mm. The amplitude of R_{yy} remains above 0.95 as L changes. The frequency-phase dashed lines corresponding to different L are almost parallel to each other in the 26–32 GHz band, indicating a stable frequency response bandwidth. Fig. 5(b) shows the effect of the oblique incidence angle of the incident EM waves on R_{yy}. At 30 GHz, within the range where the incident angle of the EM waves was less than 32°, the amplitude and phase of the reflection coefficient remained stable. When the oblique incidence angle was greater than 40°, R_{yy} underwent significant changes.

3. DESIGN OF REFLECTIVE APERTURE

The RA aperture is composed of 30 × 30 elements with a diameter of $D = 150$ mm. The forward and backward EM waves were controlled by transmissive and reflection elements, respectively. The y-polarized horn was placed at the center directly above the metasurface and vertically illuminated the aperture. Based on the performance of the transmissive and reflection elements, it is concluded that when the oblique incidence angle of the EM waves is less than 32°, the reflection

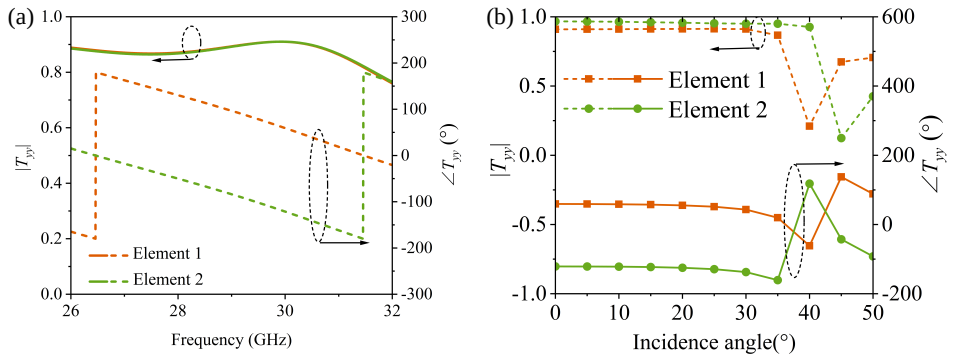

FIGURE 3. (a) T_{yy} of transmissive elements. (b) Effect of oblique incidence angle on T_{yy}.

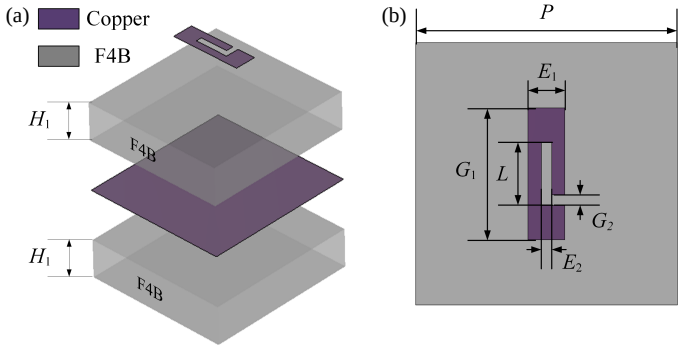

FIGURE 4. (a) Exploded view of reflective element. (b) Vertical view of reflective element. ($P = 5.00$, $E_1 = 0.70$, $E_2 = 0.20$, $G_1 = 2.50$, $G_2 = 0.20$, $H_1 = 1.40$, unit: mm).

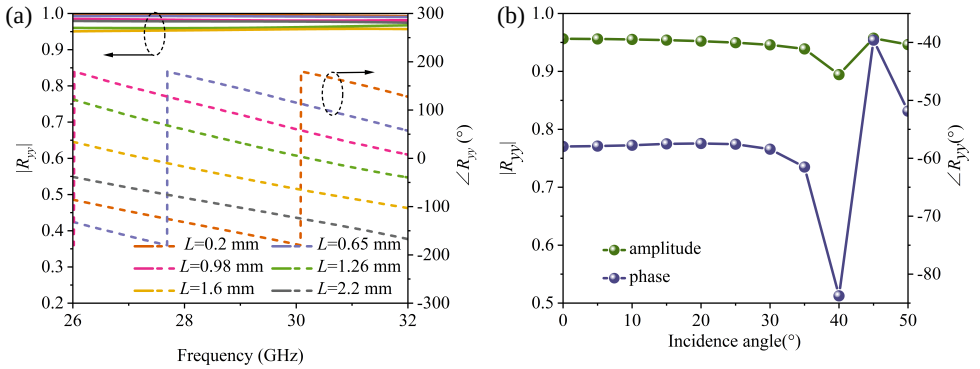

FIGURE 5. (a) R_{yy} of reflective elements. (b) Tnfluence of the oblique incidence angle of EM waves on R_{yy} ($L = 1.6$ mm).

and transmissive elements are insensitive to the incident angle. Therefore, when the focal length F is determined, the influence of the incident angle on the performance of the phase-shifting elements should be considered to reduce the error between subsequent theoretical calculations and simulation results. The relationship between focal length F and metasurface diameter D is given as

$$\theta_{i\,\max} = \tan^{-1}(0.5D/F) = 32^\circ \tag{1}$$

Thus, $F = 120$ mm is calculated.

3.1. Theoretical Phase Distribution of the Reflective Aperture

According to the phase compensation theorem and superposition method of complex reflection coefficients, the phase of the element at coordinates (x, y) on a multi-beam metasurface can be calculated by [18]

$$\phi(x,y) = -ph_{xy} + \Delta\varphi + \arg\left\{\sum_{i=1}^{g} \exp[-jk_0 p \sin\theta_i (x\cos\varphi_i + y\sin\varphi_i)]\right\} \tag{2}$$

where g is the number of beams, k_0 the free-space wavenumber, p the element period, (θ_i, ϕ_i) the radiation direction of beam i, and $\Delta\varphi$ the initial phase. $\Delta\varphi$ parameter varies within the range of 0–2π and exerts a distinct influence on the side-lobe level (SLL) and antenna gain [18]. ph_{xy} is the spatial phase delay from the feeder to the reflective aperture, which was obtained by a full-wave simulation with Computer Simulation Technology (CST) studio.

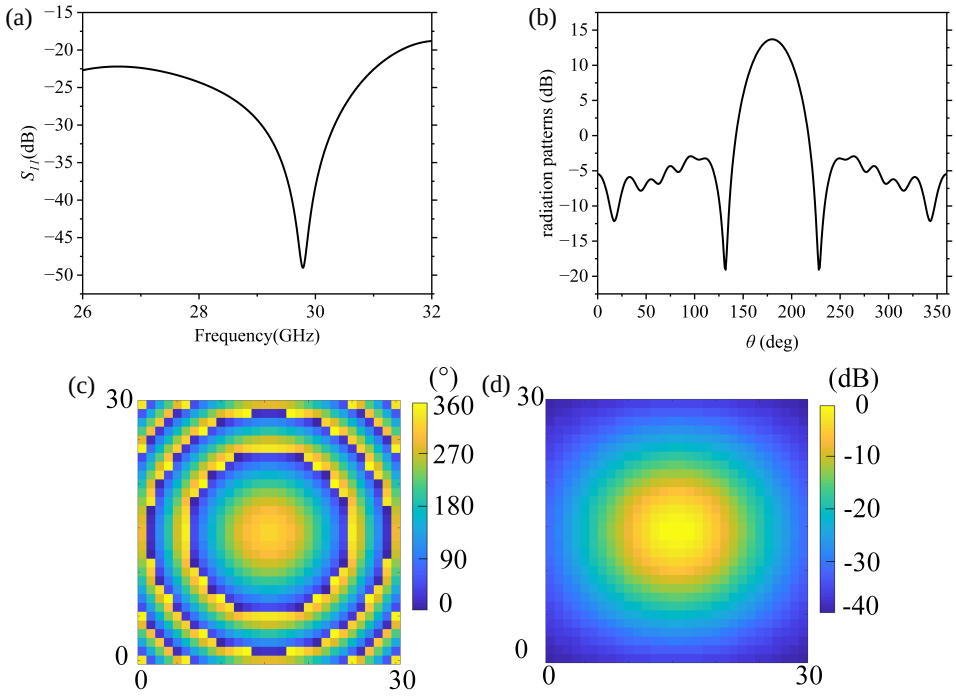

FIGURE 6. (a) Phase distribution of incident waves on the reflective aperture. (b) Amplitude distribution of incident waves on the reflective aperture. (c) Simulation result plot of the reflection coefficient for the feed horn antenna. (d) Simulation result plot of the radiation pattern for the feed horn antenna.

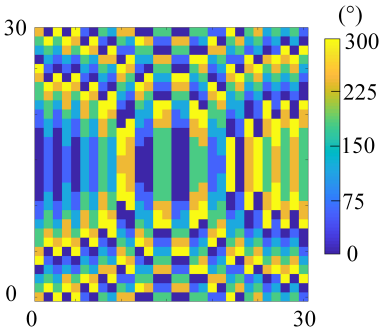

FIGURE 7. Phase distributions of metasurface apertures for dual beams.

The phase compensation was designed at a center frequency of 30 GHz in the operating band. The directions of the reflection beams were (0°, 30°) and (0°, −30°). The feed source used has good impedance matching bandwidth and directionality, as shown in Figs. 6(a) and (b). The extracted electric field distribution from the feeder to the aperture is shown in Figs. 6(c) and (d), which shows a uniform distribution in the center and most areas of the aperture, due to the joint design of the feed gain and focal-diameter ratio (F/D). The incident field phase exhibits a periodic distribution. The phase compensation scheme for the reflected dual beams calculated using Eq. (2) is theoretically shown in Fig. 7, which is the foundation of the dual-beam optimization.

3.2. Optimization of the Elements Arrangement

Because the transmissive and reflection elements do not have a polarization conversion function, the polarization of the radiation field is the same as that of the feeding horn antenna. Once the incidence field distribution on the aperture is determined, the secondary radiation field can be analyzed based on the array theory. The far-field radiation of an array aperture can be calculated as:

$$\mathbf{E}^Y(u,v) = \sum_{m=1}^{M}\sum_{n=1}^{N} \mathbf{E}^Y_{out}(n,m)e^{jn(2\pi/\lambda)d_x u}e^{jm(2\pi/\lambda)d_y v} \quad (3)$$

where $u = \sin\theta\cos\varphi$ and $v = \sin\theta\sin\varphi$ represent the elevation and azimuth angles of the entire antenna array, respectively; λ denotes the free-space wavelength; d_x and d_y represent the distances between elements in the x and y directions, respectively; $\mathbf{E}^Y_{out}(n,m)$ denotes the reflected or transmitted field of the antenna element located at position (m,n) on the aperture plane. The correlation between the incident field and $\mathbf{E}^Y_{out}(n,m)$ can be mathematically formulated as [19]

$$\mathbf{E}^Y_{out}(n,m) \cong A_{inc}(n,m)A_m(n,m)\cdot e^{j(\varphi_{inc}(n,m)+\varphi_m(n,m))} \quad (4)$$

where $A_{inc}(n,m)$ and $A_m(n,m)$ are the magnitude of the incident EM waves and reflection/transmission coefficient, respectively; $\varphi_{inc}(n,m)$ and $\varphi_m(n,m)$ denote the phase of the incident EM waves and reflection/transmission coefficient, respectively.

Because only part of the elements of the metasurface operate in the reflection mode, the RA composed of reflection and transmission elements can be considered a sparse configuration compared to a full RA antenna. For the reflected beam, the reflective elements are capable of manipulating the phase of electromagnetic (EM) waves, while providing a reflection

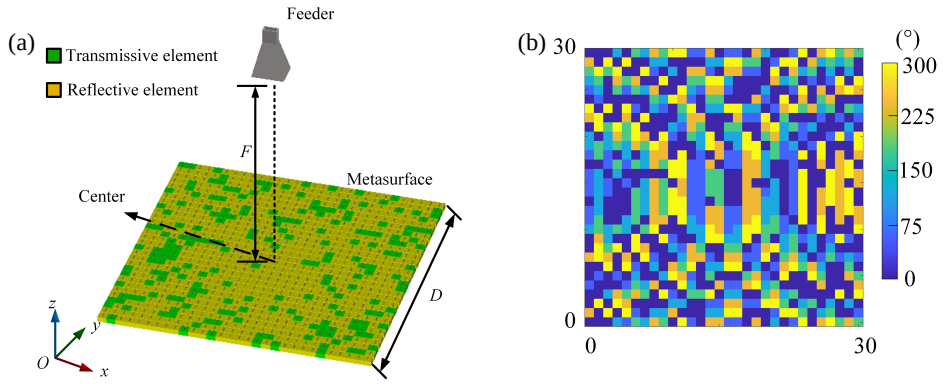

FIGURE 8. (a) Optimized arrangement of reflective and transmissive elements on reflective aperture. (b) Complete phase compensation of the metasurface.

amplitude of 1, and the transmissive elements are equivalent to dummy elements whose reflection amplitude is 0. Therefore, the optimization of the arrangement of transmission and reflection elements is transformed into the optimization of the reflective amplitude distribution of metasurfaces. Thus, the value of the reflection amplitude of each element was discretized into 0 or 1. By substituting the phase distribution required for the dual beams and the incidence field distribution in Eq. (3), the far-field radiation pattern of the dual beams can be calculated.

A genetic algorithm was used to optimize the reflective amplitude distribution to reduce the SLL of the reflected beams. The fitness function is used to evaluate the approximation degree between the current SLL and target SLL, which is expressed as

$$Fitness = |SLL_{\max} - SLL_0| \tag{5}$$

where $SLL_{\max}$ is the maximum SLL by theoretical calculation, and SLL_0 is the target side-lobe level. Then, the optimization problem of amplitude is transformed into finding the minimum value of the fitness function. Considering SLL_0 as -25 dB, the population size and mutation rate were set to 400 and 0.3, respectively. The fitness function converges after 140 iterations.

The amplitude distribution of the optimized metasurface is the same as that of the transmissive and reflective elements, as shown in Fig. 8(a). The complete phase distribution of the aperture was obtained by combining the phase distributions of the reflection and transmissive elements, as shown in Fig. 8(b). Because the transmissive element can be regarded as a reflective element with a reflection amplitude of 0 and reflection phase of any degree, the reflection phase distribution is uniform for the reflected beam.

4. RESULTS AND DISCUSSION

To verify the effectiveness of the proposed method, a prototype is fabricated, as shown in Fig. 9. The metasurface was fabricated via printed circuit board (PCB) technology and subsequently fastened using plastic screws with a diameter of 2 mm. To mitigate the difficulties associated with fabrication and processing, the phase variations of the reflective unit were categorized into six distinct types. The horn antenna was placed perpendicular to the aperture and pointed towards the center of the reflectarray.

The radiation performance of the prototype was measured, and the simulations and measurements showed good consistency. The normalized radiation patterns of the metasurface antenna at 30 GHz are shown in Fig. 10. The unoptimized RA means the traditional full RA without dummy transmissive elements, which has an SLL of -15.7 dB, while the SLL of the optimized dual beams is less than -19.0 dB.

The SLL was effectively suppressed by optimizing the arrangement of transmission and reflection elements. Although some electromagnetic energy may be transmitted backward through the transmissive elements, the front-to-back ratio (FBR) of the entire antenna remains at 27 dB. Because there is no targeted phase compensation for the transmitted beam, a strong radiation is not generated in the backward direction. Meanwhile, the cross-polarization level was less than -25.0 dB.

According to [20], the aperture efficiency (AE) of each beam of the dual-beam antenna can be calculated as [20]:

$$AE = G \times \frac{\lambda^2}{4\pi S \cos^2 \theta_r} \tag{6}$$

where G is the beam gain, S the physical area of the aperture, and θ_r the beam deflection angle. The AE of the dual-beam antenna was obtained by adding the aperture efficiencies of each beam.

The gain and AE of the dual-beam metasurface antenna are shown in Fig. 11. The beam with a deflection of 30° gets a peak gain of 26.3 dBi at 30.5 GHz, and its 3-dB gain bandwidth is 15.4% (27 GHz ∼ 31.5 GHz). The beam with a deflection of $-30°$ reached a maximum gain of 25.8 dBi at 29.5 GHz, and its 3-dB gain bandwidth was 13.8% (27 GHz ∼ 31 GHz). The measured AE reaches a peak of 38.9% at 29.5 GHz, corresponding to gains of 26.2 dBi and 25.8 dBi for beams deflected at 30° and $-30°$, respectively. The difference in the gain of the two beams is mainly due to the asymmetric aperture structure caused by the irregularly arranged elements.

Table 1 compares the proposed antenna with previous metasurface-based RAs. This configuration effectively

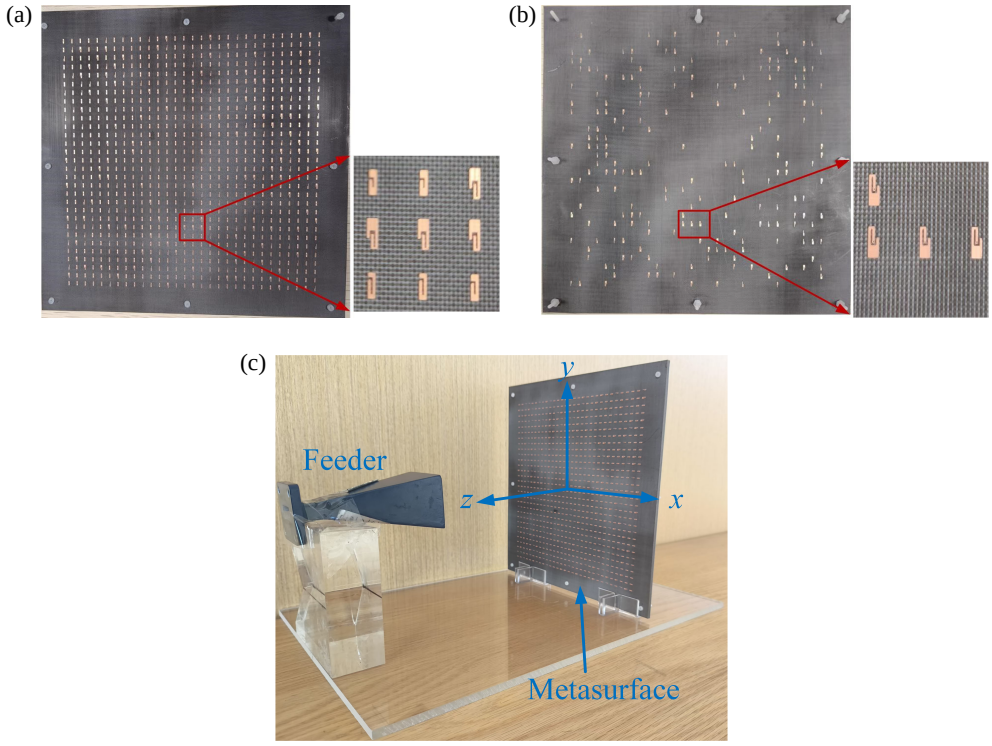

FIGURE 9. (a) Top view of the metasurface aperture. (b) Bottom view of metasurface PCB. (c) Prototype antenna system.

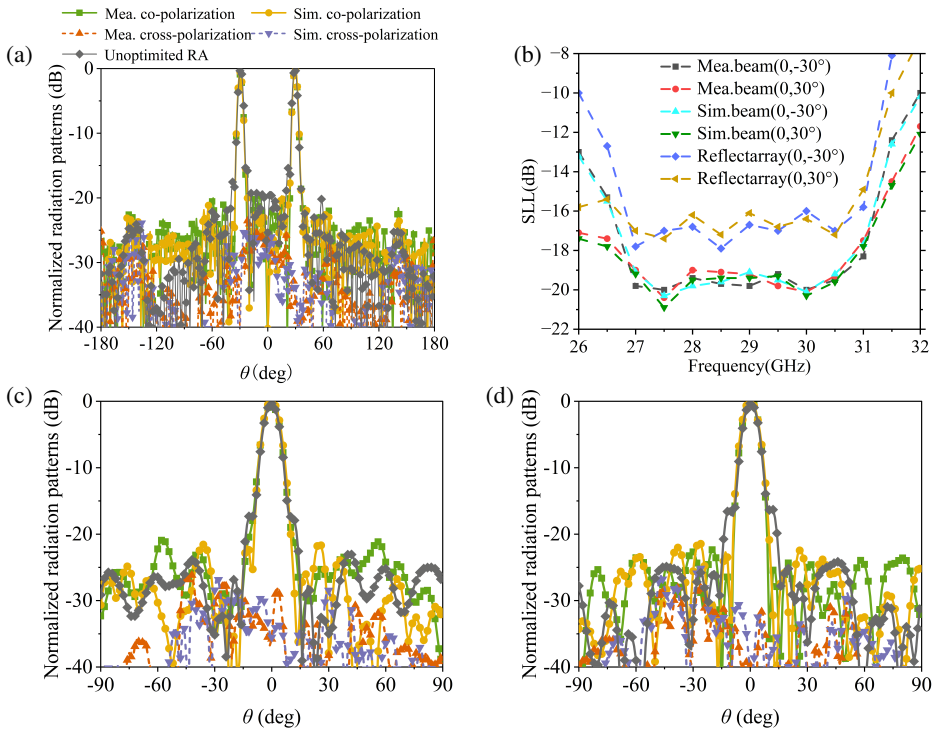

FIGURE 10. (a) Phi $= 90°$ plane of the dual beams. (b) SLLs of the dual beams. (c) Orthogonal plane of the beam with a deflection of $-30°$. (d) Orthogonal plane of the beam with a deflection of $30°$.

mitigates the side lobes of the antenna while maintaining low cross-polarization levels. Compared with other low side-lobe antennas based on polarization conversion amplitude-modulated metasurfaces, the proposed antenna utilizes reflective units and transmissive units to regulate the amplitude of the reflected wave, without converting the co-polarized wave into a cross-polarized wave, thus exhibiting a lower cross-polarization level. The proposed antennas have

TABLE 1. Comparison with the previous metasurface-based RAs.

Ref.	Freq. (GHz)	Aperture Size (mm)	Beams	SLL (dB)	AE (%)	X-pol. Levels (dB)	BW
[5]	12	200 * 200	3	−16.0	NA	NA	19.5% (3 dB)
[6]	10	220 * 220	2	−13.6	16.2	−30	3.5% (3 dB)
[14]	19	180 * 180	2	−19.6	36.8	NA	NA
[16]	3	160 * 160	2	NA	7/14	NA	6.7/9.3 (1 dB)
[21]	33	140 * 140	2	−14.0	20	−20.0	28.6% (2 dB)
[22]	10.8/14.3	170 * 170	2	−10/−10	21.6/20.6	−20/−25	7.5%/5.7% (1 dB)
This work	30	150 * 150	2	−19.0	38.9	−25.0	13.8% (3 dB)

* X-pol. levels are cross-polarization levels. * BW is gain bandwidth. * NA: not available.

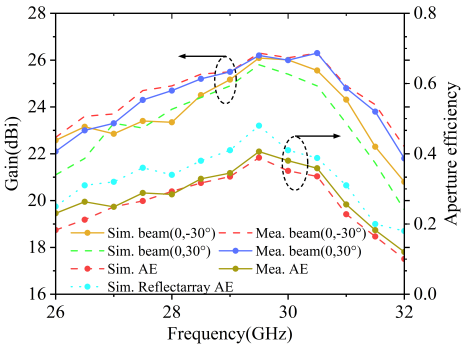

FIGURE 11. Gain and AE of the dual-beam RA.

the advantages of two beams and wide radiation range. The SLL of the dual beams radiated by the designed antenna is low, resulting in strong anti-interference capabilities. Peak AE has significant advantages, enabling the proposed RA to provide a better gain. Furthermore, the proposed design eliminates the need for complex phase control or reconfiguration mechanisms, making it more suitable for millimeter-wave multi-target radar scenarios.

5. CONCLUSION

High-gain dual-beam antennas have significant application value for wireless communication and multi-target radar systems, and the design challenge lies in achieving an optimal balance between gain and side lobes under limited physical aperture. A dual-beam metasurface antenna is proposed, which combines reflectarray and sparse array theories to achieve a high gain and low SLL. Compared with the traditional low side-lobe RA based on the polarization conversion amplitude modulation metasurface, the proposed RA draws inspiration from the concept of sparse arrays and uses transmissive elements as dummy elements, which reduces the side-lobe levels without increasing the cross-polarization levels. The arrangements of the metasurface elements were globally optimized using the GA method, which are beneficial for the suppression of SLL. The dual beams of the prototype measurement have a gain 26.0 dBi, SLL −20 dB, and 3-dB gain bandwidth of 13.8%. The proposed method is also applicable to the design of reflective array antennas with low SLL and beams.

ACKNOWLEDGEMENT

This work was supported in part by the China Postdoctoral Science Foundation under Grant 2022MD723726.

REFERENCES

[1] Zhang, C., Y. Luo, Y. He, N. Yan, and K. Ma, "Multi-beam quad-polarized transmit-array antenna with arbitrary radiation direction for vehicle communication via generalized phase superposition," *IEEE Transactions on Antennas and Propagation*, Vol. 73, No. 3, 1414–1425, 2025.

[2] Guo, X., Y. Guo, Y. Luo, and Y. Yang, "Full-space transmission-reflection-integrated metasurface for multibeam generation on orthogonal planes," *IEEE Transactions on Microwave Theory and Techniques*, Vol. 73, No. 10, 8199–8209, 2025.

[3] Malleboina, R. and D. Sarkar, "Single-feed near-field excited quad-beam metasurface antenna," *IEEE Antennas and Wireless Propagation Letters*, Vol. 24, No. 1, 137–141, 2025.

[4] Nayeri, P., F. Yang, and A. Z. Elsherbeni, "Design and experiment of a single-feed quad-beam reflectarray antenna," *IEEE Transactions on Antennas and Propagation*, Vol. 60, No. 2, 1166–1171, 2012.

[5] Liu, X., Z. Yan, E. Wang, X. Zhao, T. Zhang, and F. Fan, "Multibeam forming with arbitrary radiation power ratios based on a conformal amplitude-phase-controlled metasurface," *IEEE Transactions on Antennas and Propagation*, Vol. 71, No. 4, 3707–3712, 2023.

[6] Song, L.-Z., X. Wang, and P.-Y. Qin, "Single-feed multi-beam conformal transmitarrays with phase and amplitude modulations," *IEEE Antennas and Wireless Propagation Letters*, Vol. 21, No. 8, 1669–1673, 2022.

[7] Tong, X., W. Zeng, Y. Li, F. Wu, Z. H. Jiang, R. Sauleau, and W. Hong, "A dual-band dual-circularly polarized transmit-array antenna and its application for four-color scheme multi-beam generation," *IEEE Transactions on Antennas and Propagation*, Vol. 72, No. 11, 8511–8526, 2024.

[8] Yang, W., K. Chen, J. Zhao, T. Jiang, and Y. Feng, "Frequency-multiplexed spin-decoupled metasurface for low-profile dual-band dual-circularly polarized transmitarray with independent beams," *IEEE Transactions on Antennas and Propagation*, Vol. 72, No. 1, 642–652, 2024.

[9] Wu, L.-X., N. Zhang, K. Qu, K. Chen, T. Jiang, J. Zhao, and Y. Feng, "Transmissive metasurface with independent amplitude/phase control and its application to low-side-lobe metalens antenna," *IEEE Transactions on Antennas and Propagation*, Vol. 70, No. 8, 6526–6536, 2022.

[10] Lou, Q. and Z. N. Chen, "Sidelobe suppression of metalens antenna by amplitude and phase controllable metasurfaces," *IEEE Transactions on Antennas and Propagation*, Vol. 69, No. 10, 6977–6981, 2021.

[11] Sun, M., K. Xu, Y. Yang, S. Chen, T. Wang, D. Yu, X. Yu, and G. Wang, "Folded transmitarray antenna via independent amplitude/phase control with low side-lobe for millimeter-wave communication," *IEEE Transactions on Circuits and Systems II: Express Briefs*, Vol. 71, No. 4, 2004–2008, 2024.

[12] Yin, L., C. Jin, Q. Lv, B. Zhang, K. Cao, P. Zhang, and Z. Xue, "Amplitude and phase independently adjustable transmitarray aperture and its applications to high gain and low sidelobe antenna," *IEEE Transactions on Antennas and Propagation*, Vol. 70, No. 6, 4498–4506, 2022.

[13] Li, H.-P., G.-M. Wang, T. Cai, J.-G. Liang, and X.-J. Gao, "Phase-and amplitude-control metasurfaces for antenna mainlobe and sidelobe manipulations," *IEEE Transactions on Antennas and Propagation*, Vol. 66, No. 10, 5121–5129, Oct. 2018.

[14] Zhang, P., W. Zhang, X. Chen, G. Han, J. Su, and R. Yang, "Low-sidelobe dual-beam antenna based on metasurface with independently regulated amplitude/phase," *IEEE Antennas and Wireless Propagation Letters*, Vol. 22, No. 10, 2382–2386, Oct. 2023.

[15] Liu, Q., X.-W. Chen, W.-B. Niu, M.-Y. Xia, and W.-M. Zhang, "Low sidelobe dual-beam metasurface antenna based on taylor distribution and digital filtering methods," *IEEE Antennas and Wireless Propagation Letters*, Vol. 24, No. 4, 1003–1007, 2025.

[16] Liu, S. L., X. Q. Lin, Y. H. Yan, and Y. L. Fan, "Generation of a high-gain bidirectional transmit-reflect-array antenna with asymmetric beams using sparse-array method," *IEEE Transactions on Antennas and Propagation*, Vol. 69, No. 9, 6087–6092, 2021.

[17] Zhang, H., W. Wu, Q. Cheng, Q. Chen, Y.-H. Yu, and D.-G. Fang, "Reconfigurable reflectarray antenna based on hyperuniform disordered distribution," *IEEE Transactions on Antennas and Propagation*, Vol. 70, No. 9, 7513–7523, 2022.

[18] Yang, H., F. Yang, S. Xu, Y. Mao, M. Li, X. Cao, and J. Gao, "A 1-bit 10×10 reconfigurable reflectarray antenna: Design, optimization, and experiment," *IEEE Transactions on Antennas and Propagation*, Vol. 64, No. 6, 2246–2254, 2016.

[19] Luo, W., L. Luo, X. Wang, M. Wang, and H. Zhang, "Dual-band dual-linearly polarized multibeam transmit-reflect-array antenna with independent beams control," *Alexandria Engineering Journal*, Vol. 127, 34–42, 2025.

[20] Xu, P., L. Li, R. Li, and H. Liu, "Dual-circularly polarized spin-decoupled reflectarray with FSS-back for independent operating at Ku-/Ka-bands," *IEEE Transactions on Antennas and Propagation*, Vol. 69, No. 10, 7041–7046, 2021.

[21] Yin, J., Q. Lou, H. Wang, Z. N. Chen, and W. Hong, "Broadband dual-polarized single-layer reflectarray antenna with independently controllable 1-bit dual beams," *IEEE Transactions on Antennas and Propagation*, Vol. 69, No. 6, 3294–3302, 2021.

[22] Sun, Y., S. Liao, and H. Zhu, "Dual-frequency dual-beam reflectarray based on frequency-division duplexing reflection phase-shifting element," *IEEE Antennas and Wireless Propagation Letters*, Vol. 24, No. 12, 4570–4574, 2025.